Applied Catalysis B: Environmental 86 (2009) 127–136

Contents lists available at ScienceDirect

Applied Catalysis B: Environmental

journal homepage: www.elsevier.com/locate/apcatb

An investigation of the performance of catalytic aerogel filters

Shengli Cao [a], King Lun Yeung [a,*], Joseph K.C. Kwan [b], Percy M.T. To [b], Samuel C.T. Yu [b]

[a] Department of Chemical Engineering, Hong Kong University of Science and Technology, Clear Water Bay, Kowloon, Hong Kong, PR China
[b] Health, Safety and Environment Office, Hong Kong University of Science and Technology, Clear Water Bay, Kowloon, Hong Kong, PR China

ARTICLE INFO

Article history:
Received 3 April 2008
Received in revised form 7 July 2008
Accepted 11 August 2008
Available online 29 August 2008

Keywords:
Titania–silica aerogel
Nano-TiO_2
Photocatalyst
Antimicrobial
Aerosol

ABSTRACT

Gas permeable, photoactive and crack-free titania–silica aerogels of high titanium content (i.e., up to Ti/Si = 1) were prepared by two-steps acid–base catalyzed method involving an acid-catalyzed prehydrolysis of silicon alkoxide followed by a base-catalyzed hydrolysis/condensation reactions with a chelated titania precursor. The prepared titania–silica aerogels displayed good mechanical strength (>30 kN m^{-2}), large surface area (>550 m^2/g), mesoporous structure (8–11 nm) and good gas permeation. The porous aerogels trap and filter airborne particulates and the titania–silica aerogel have a fair performance for aerosol (65%) and bioaerosol (94%) filtrations. The photoactive anatase nano-TiO_2 crystallized within the aerogel displays an order of magnitude higher reaction rate for UVA photooxidation of trichloroethylene compared to commercial Degussa P25 TiO_2. The bactericidal activity of the titania–silica aerogel for *Bacillus subtilis* cells under UVA was also six orders of magnitude better.

1. Introduction

Titanium dioxide (TiO_2) being inexpensive remains a popular photocatalyst [1]. It has a remarkably high photoactivity under near-UV irradiation and is shown to effectively remedy a variety of airborne organic pollutants [2–4]. Researches show that UV irradiated TiO_2 could deactivate and kill airborne microorganisms including bacteria and spores [5–8]. An assortment of TiO_2 materials including TiO_2 aerosols [9,10], aerogels [11–15], nanorods [16,17], nanotubes [18–21], nanocrystals [22–26] and mesoporous materials [27–30] had been prepared in recent years and tested for photocatalytic activity. TiO_2 aerogels prepared by sol–gel method and supercritical drying are characterized by nanometer-sized crystalline particles, high porosity, large surface area and pore volume [11–15] that are responsible for their superior activity for photooxidation of organics such as salicylic acid [14] and benzene [15].

A self-supporting TiO_2 aerogel block would be an ideal catalytic filter. However, the weak Ti–O–Ti network made it difficult to prepare freestanding titania aerogel. Instead, Yoda et al. [31,32] prepared freestanding titania–silica aerogels by impregnating titania precursor into silica alcogels before supercritical drying. However, the aerogels prepared by this method suffered from non-uniform titania distribution. Kim and Hong [33] used NH_4OH/NH_4F catalyzed cohydrolysis of acetalacetone modified tetrabutyl orthotitanate and tetraethyl orthosilicate to prepare crack-free titania–silica aerogel with Ti/Si < 0.1. Our group reported [34–37] the preparation of freestanding, crack-free titania–silica aerogels of high Ti content (i.e., Ti/Si = 1) that display good permeability to gases [35] unlike traditional aerogels that were reported to be impervious to gas flow [38,39]. Crystallized within the porous silica network are photoactive anatase TiO_2 nanoparticles that gave the titania–silica aerogels their excellent photocatalytic activity [34]. Trapped within the porous aerogel, the nano-TiO_2 is very stable and could withstand high temperature without sintering. The aerogel matrix also prevents the accidental release of nano-TiO_2 into the environment and thus minimizes the potential adverse impact of the nanomaterial to health and environment.

This work examines the synthesis of gas permeable and photoactive titania–silica aerogel blocks by two-steps, acid–base catalyzed method. The physical, chemical and textural properties of the prepared aerogels were characterized and compared to samples prepared by the traditional acid and base-catalyzed cohydrolysis methods. The new titania–silica aerogels (Ti/Si = 0.2, 0.5 and 1) were tested for gas transport and diffusion, aerosol and bioaerosol filtrations, photocatalytic oxidation of airborne trichloroethylene (TCE) and antibacterial activity against *Bacillus subtilis* cell.

2. Experimental

2.1. Preparation of titania–silica and silica aerogel

The titania–silica aerogels were prepared by a two-step, acid–base catalyzed procedure [34–36]. The chemical preparation and

* Corresponding author. Tel.: +852 2358 7123; fax: +852 2358 0054.
E-mail address: kekyeung@ust.hk (K.L. Yeung).

0926-3373/$ – see front matter © 2008 Elsevier B.V. All rights reserved.
doi:10.1016/j.apcatb.2008.08.019

alcogel synthesis were carried out in a dry, nitrogen box. Tetramethyl orthosilicate (TMOS, 98%, Aldrich) was dissolved in ethanol (99.9%, Merck) and prehydrolyzed with a dilute nitric acid solution (Fisher Scientific) at 323 K for 90 min under vigorous stirring to give a solution with a molar ratio of 1 TMOS:2 H_2O:0.005 HNO_3:10.2 C_2H_5OH. In a second solution, titanium isopropoxide (TIP, 98+%, Acros) in ethanol was reacted with acetylacetone (acac, 99+%, Sigma–Aldrich) in 1:1 mol ratio to give a solution containing x TIP:x acac:2 C_2H_5OH. Measured amounts of the two solutions were mixed together and a dilute ammonia solution (Fisher Scientific) was added to complete the reaction. Depending on the Ti/Si ratio (i.e., 0.1, 0.2, 0.5 and 1) the final mixture has a molar ratio of 1 TMOS:x TIP:x acac:$4 + 2x$ H_2O:0.005 HNO_3:0.07 NH_3:12.25 C_2H_5OH. The gelation time depends on the titanium content of the samples and the resulting alcogels were aged for 10 days. After ageing, the wet alcogels were dried by ethanol supercritical drying. The alcogel (5 cm^3) was placed in a glass sample holder (20 cm^3) and immersed in 10 ml ethanol. The sample holder assembly was sealed in the stainless steel autoclave (150 cm^3) with an additional 70 ml ethanol. The autoclave was heated at 60 K min^{-1} to 553 K, while keeping the autoclave pressure below 10.6 MPa. During supercritical drying, the ethanol vapor was released at a rate of roughly 4 kPa min^{-1} at a constant temperature. The autoclave was purged with 10 cm^3 min^{-1} dry nitrogen for an hour, before cooling down to the ambient temperature. The aerogel sample was removed for inspection before calcination in air at 723 K for 1 h in a carbolite furnace at constant heating and cool rates of 30 K h^{-1}.

The silica aerogel was prepared for comparison. The TMOS in ethanol was mixed with dilute ammonia to give a solution with a mole ratio of 1 TMOS:4 H_2O:0.065 NH_3:12.25 C_2H_5OH. The silica alcogel was aged for 10 days before ethanol supercritical drying, and was calcined at 723 K to obtain the final aerogel. We also prepared titania–silica aerogel by a one-step, base-catalyzed, co-hydrolysis procedure similar to that described by Kim and Hong [33] but using titanium isopropoxide and without NH_4F. The TIP dissolved in ethanol was first reacted with an equimolar acetylacetone in ethanol before mixing with TMOS. A dilute ammonia solution was then added under vigorous mixing to give a final composition of 1 TMOS:x TIP:x acac:$4 + 2x$ H_2O:0.065 NH_3:12.25 C_2H_5OH. The CO_2 supercritical drying was carried out after the alcogels were aged for 10 days according to procedure described in the recent work [34–36].

2.2. Physical and chemical characterization of aerogels

The calcined aerogels were examined for defects and samples were prepared for inspection under optical (Olympus, BH2-MJLT) and scanning electron microscope (SEM, JEOL JSM 6300 F). A piece of the aerogel was mounted on the aluminum specimen stub by conducting graphite adhesive and sputter coated with a thin layer of gold (ca. 10 nm) to decrease sample charging during the SEM imaging. A second piece of sample was used in compressive strength test in an Instron 5567 Tensile/Compression Tester. The remainder of the aerogel sample was ground into powder for X-ray diffraction and nitrogen physisorption analysis. The aerogel powder was placed in an aluminum sample holder and analyzed by Philips PW 1830 powder X-ray diffractometer. The diffractograms were recorded with Cu Kα X-ray over a 2θ range of 20–60° with a step of 0.05°. Nitrogen physisorption of the powder samples was carried out in a Coulter SA 3100 to determine the specific surface area, pores size distribution and pore volume of the aerogel. The surface area of the crystallized anatase TiO_2 in the mixed-oxides aerogels was determined by 2-propanol dehydration reaction according to the procedure described by Hanprasopwattana et al. [40]. Five reference anatase TiO_2 of known surface area (i.e., 15–90 m^2 g^{-1}) were prepared [41,42] for the purpose of calibration. The catalyst samples were pretreated in helium at 373 K for an hour prior to the dehydration reaction at 533 K.

The gas permeation and diffusion experiments were done in a Wicke–Kallenbach cell [34] with the aerogel block mounted and sealed in the sample holder with silicone glue. The oxygen permeation across the aerogel was determined by flowing oxygen against one face of the aerogel and measuring the flux and pressure drop across the sample with bubble flow meter and manometer. The oxygen diffusion at different temperatures was conducted at 101 kPa with 10% O_2/He gas mixture flowing at 50 standard cm^3 min^{-1} (sccm) along one face of the aerogel block and 50 sccm helium across the other face. The gas composition of the exit streams was analyzed by a gas chromatograph (HP 6890) equipped with a CRT1 column (Alltech) and a thermal conductivity detector. The ultrahigh purity oxygen and helium gases were purchased from Hong Kong Specialty Gases Co. Ltd and the 10% O_2/He mixture was supplied by Chun Wang Industrial Gases (CWIG).

The bulk and surface compositions of the aerogel powder were determined by JEOL JSX-3201Z X-ray fluorescence spectroscopy (XRF) and Physical Electronics PHI 5600 X-ray photoelectron spectroscopy (XPS), respectively. The XPS analysis was done with an Al monochromatic X-ray at a shallow angle to sample the topmost surface layer. The aerogel powder was also analyzed by Perkin–Elmer Fourier transformed infrared spectrometer. The UV penetration in aerogel sample was determined using the method described by Dreyer [43]. A 1.8 mg of the finely ground titania–silica aerogel powder was vigorously mixed and suspended in 3 ml silica solution containing 1 TMOS:4 H_2O:0.065 NH_3:12.25 C_2H_5OH and followed by a rapid gelation (i.e., <30 min). After ageing and ethanol supercritical drying, a finely dispersed titania–silica powder in cylindrical aerogel block was obtained. The transmission of ultraviolet light at a wavelength of 365 nm was measured by Perkin–Elmer Lambda 20 UV/VIS spectrophotometer.

2.3. Performance of catalytic aerogel filters

Aerosol filtration measurements were carried out in the experimental set-up shown in Fig. 1a. Sub-micron poly-dispersed oil mist aerosol (Poly Alpha Olefin) with a specified count mean diameter of 0.28 μm was generated by ATI TDA-4B aerosol generator (Air Techniques) at a concentration of 2500 μg l^{-1}. The aerosols were uniformly circulated in a fog chamber by a set of fans. Air was drawn using a pair of SKS AirChek^{2000} air sampling pumps. The first set of pump filtered the air through an aerogel block sealed in a plastic holder at constant air flow of 200 sccm for 1 h. A SKS hydrophobic PVC filter located downstream collects the oil droplets that penetrated the aerogel. The second set of pump filtered the air through the SKS PVC filter and provided reference data on the concentration of aerosol mist in the fog chamber. The two PVC filters were weighed to determine the total and penetrated aerosols, from which the filtration efficiency could be calculated. The air sampling rate was calibrated at the start of the experiment using the BIOS International's DryCal® DC-Lite Primary Flow Meter.

Bioaerosol filtration was done for natural bioaerosol using the experimental set-up shown in Fig. 1b. The experiments were conducted at the open-air, campus atrium. The aerogel block was mounted and sealed in a stainless steel holder and placed as a filter in a SKC Biostage® bioaerosol impactor. Air was drawn through the aerogel with an Air CADET® pump to impact on a Tryptic soy agar (TSA, Oxoid) plate. The TSA plate was prepared by dissolving tryptic soy agar in 500 ml distilled water in a 1 l conical flask. The solution was autoclaved (Hirayama, HA-300P) at 394 K for 15 min, and cooled down to 333 K. Twenty-five milliliters of the solution

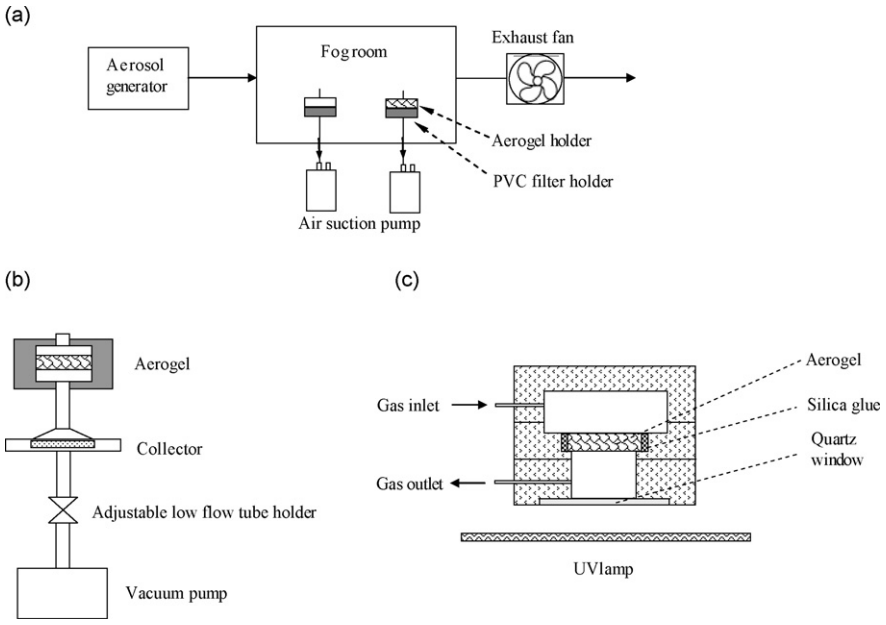

Fig. 1. Schematic drawings of (a) the aerosol filtration test set-up, (b) bioaerosol filtration test unit and (c) aerogel photoreactor.

was transferred to 100 mm Petri dishes and allowed to gel. The plates were flamed to sterilize the surface and remove bubbles, before cooling in a biosafety cabinet. Aseptic technique was followed during the assembly of the experimental set-up to avoid contamination. Assembly was done in a biosafety cabinet which had been disinfected by UVC disinfection for 30 min. The flexible tubing connecting the pump to the bioaerosol impactor was sterilized and all the surfaces were wiped cleaned with ethanol. After placing the TSA plate in the bioaerosol impactor, the aerogel filter and vacuum pump were connected as shown in Fig. 1b. The pump was pre-calibrated to deliver 200 sccm air flow using a flow meter. A sampling time of 2 h was used and a parallel set of bioaerosol impactor was used to obtain a measurement of the bioaerosol concentration in the air. The TSA plate was sealed immediately after sampling and incubated in Gallenkamp incubator at 310 ± 0.1 K for 24 h to determine the filtration efficiency of the aerogel samples.

Photocatalytic oxidation (PCO) activity of the aerogel filters was tested in an aerogel photoreactor shown in Fig. 1c [35]. The photoreactor consists of three machined flanges assembled to form the reactor shown in the schematic drawing. The upper flange contained an inlet for reactant feed. The center flange that held the cylindrical aerogel block is interchangeable with that of the Wicke–Kallenbach cell used for gas permeation and diffusion experiments. The bottom flange consists of a quartz window for UV illumination and an outlet for the exit gas. The aerogel filters were pretreated by ozone (i.e., 11 vol.% O_3/O_2 mixture) under UVA illumination (710 $\mu W/cm^2$) to prevent catalyst deactivation. Trichloroethylene (TCE, 99.5%, Aldrich) was fed by a syringe pump (kdScientific 100) and mixed with the dry synthetic air (22% O_2, Chun Wang Industrial gases (HK) Ltd.) before entering the photoreactor. The air was metered by an electronic mass flow controller (Sierra, Smart-Trak). The reactant mixture flows through the aerogel block irradiated by a single fluorescent black lamp (UVA, 365 nm, Philips 6W) and exits the reactor to an on-line gas chromatograph (GC, HP 6890) equipped with thermal conductivity and flame ionization detectors. A 10% CarboWax 20M on 80/100 Chromosorb W-HP column was used for the GC analysis. The reaction was maintained at room temperature (i.e., 298 ± 4 K) for the study.

Bactericidal properties of the aerogel filters were tested for *B. subtilis* (Carolina Biological Supply, 15-5065A) and natural bioaerosol (i.e., airborne bacteria). The aerogel samples were ground into a fine powder using mortal and pestle. The powder was dispersed in ethanol by sonication and 2 ml of the suspension spread on 10 mm Petri dish to form a thin adherent film. The film was dried in an oven at 333 K overnight and sterilized before use. The stock *B. subtilis* cells were kept on tryptone soya agar (TSA, Oxoid) plate (Difco) at 4 °C. The bacteria cells were revitalized by sub-culturing a loopful of inoculum in 10 ml of sterile Oxoid nutrient broth in a culture tube with gentle shaking in a Gallenkamp incubator at 310 ± 0.1 K and 80 rpm for 18 h. The viable cell concentration was determined by plate counting technique on TSA plates after a serial dilution. A 100 μl of 10^7 cm^{-3} bacteria suspension was placed in contact with both coated and uncoated Petri dishes at ambient condition (296 ± 2 K, 70% R.H.) in a biosafety cabinet (NuAire, Nu-425-400E). The coated Petri dishes were exposed to UVA light (365 nm, 2650 $\mu W/cm^2$) for fixed irradiation times of 5, 15 and 30 min. A 3 ml sterile nutrient broth (Nutrient broth no. 2, Oxoid) was added and the Petri dishes were gently shaken for 10 min. A 100 μl aliquots were then taken from both coated and uncoated Petri dishes and separately cultured on TSA plates for 24 h at 310 ± 0.1 K to give the viable bacteria counts.

The viable bacteria trapped in the aerogel filter after the bioaerosol filtration test was enumerated. The aerogel block was removed from the holder and gently broken into powder. The powder was divided into four equal portions and spread evenly on 10 mm Petri dishes and irradiated with UVA (365 nm, 2650 $\mu W/cm^2$) for 0, 0.5, 2 and 12 h. After irradiation, the powder was transferred to an eppendorf tube containing 1 ml sterilized nutrient broth and mixed with vortex stirrer for 10 min. A 100 μl aliquot was cultured on TSA plates and the number of viable bacteria was counted after incubating the plates for 24 h at 310 ± 0.1 K.

3. Results and discussions

3.1. Silica and titania–silica aerogels

Although crack-free, silica aerogels are routinely made [44–46], the preparation of titania and titania–silica aerogels is more

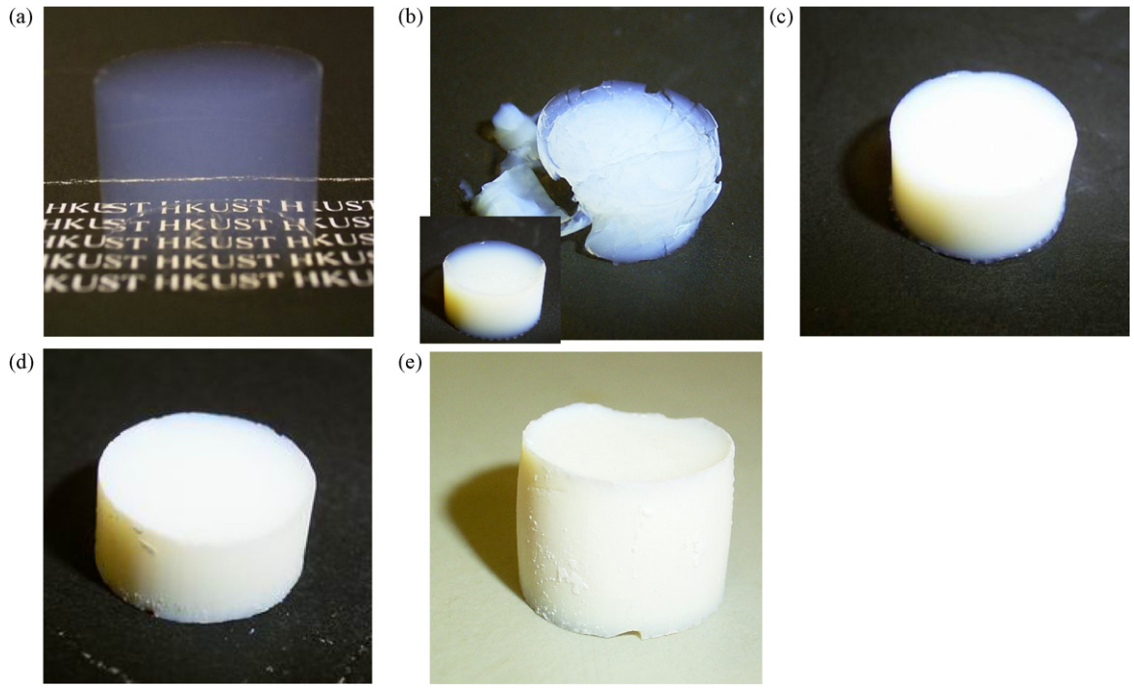

Fig. 2. Photographs of (a) silica (S_HT) and (b)–(e) titania–silica aerogels after ethanol supercritical drying and high-temperature air calcination. The titania silica aerogels contain (b) Ti/Si = 0.1 (TS01), (c) Ti/Si = 0.2 (TS02), (d) Ti/Si = 0.5 (TS05) and (e) Ti/Si = 1 (TS1) were prepared by the two-step, acid–base method.

difficult because of poor network strength [47–49]. Fig. 2 gives a pictorial summary of the titania–silica aerogels prepared by the two-step, acid–base catalyzed procedure. The aerogels were treated by ethanol supercritical drying and calcined in air at 723 K. The silica aerogel shown in Fig. 2a was prepared by a base-catalyzed route. Crack-free, titania–silica aerogel blocks were obtained after ethanol supercritical drying for samples with Ti/Si ratio of up to 1. Alcogels with Ti/Si > 1 produced mainly aerogel powder after supercritical drying. With the exception of the TS01 aerogel (Ti/Si = 0.1), all the aerogel samples remained crack-free after the high temperature air calcination. Compressive strength tests indicated that the silica aerogel can withstand 41 kN m^{-2}, while titania–silica aerogels with Ti/Si = 0.2 and 1 are able to survive compressive pressure of up to 40 and 28 kN m^{-2}, respectively. The above observations are valid over more than three dozens samples prepared for the study. The prepared titania–silica aerogels were compared with the literature data on aerogels prepared by acid-catalyzed cohydrolysis method reported by Baiker and coworkers [50,51]. A second set of titania–silica aerogels was prepared by a base-catalyzed co-hydrolysis method modified from the procedure first described by Kim and Hong [33]. The new preparation avoided the use of NH_4F and employed CO_2 supercritical drying. Except for the sample with a low titanium loading, the prepared aerogels exhibited severe crack formation consistent with the observation of Kim and Hong [33].

Fig. 3a plots the surface and bulk titanium contents of the aerogels prepared by these three methods. The surface titanium of the prepared samples was analyzed by XPS and the bulk titanium content was determined by XRF. The higher reactivity of the titanium alkoxide precursors compared to the silicon alkoxides [52] results in a non-uniform core-shell structure [50,53]. The figure shows that both the acid and base-catalyzed cohydrolysis methods produce titania–silica aerogels with surface titanium content less than half of the bulk concentration (i.e., $Ti_S/Ti_B \leq 0.50$). This is in spite of using acetylacetone chelate to slow down the reaction of the titanium alkoxide. The titania–silica aerogels obtained by the two-step, acid–base catalyzed procedure display higher surface titanium content (i.e., $Ti_S/Ti_B \sim 0.75$) as shown in Fig. 3a. Indeed, acid prehydrolysis of silicon alkoxide (i.e., TMOS) was reported by Baiker and coworkers [51] to help increase the surface titanium content of titania–silica aerogels. The infrared spectra of the titania–silicon aerogels prepared by the three synthesis methods are shown in Fig. 3b. There is no appreciable difference in the infrared bands between samples prepared by acid and base catalyzed cohydrolysis methods (cf. Fig. 3b-[1] and [2]) and the peak at ca. 960 cm^{-1} in the spectra, representing Si–O–Ti connectivity, is similar for the two aerogels. This infrared band appears weaker for the aerogel prepared by the new method (Fig. 3b-[3]) and could be explained by the crystallization of anatase TiO_2.

The textural properties of the titania–silica aerogels including total BET surface area (Fig. 3c), percent surface area from micropores (Fig. 3d), average pore diameter (Fig. 3e) and total pore volume (Fig. 3f) are compared for the three synthesis methods. It is clear that the synthesis and composition have an enormous impact on the textural properties of the prepared aerogel. The titania–silica aerogels prepared by Baiker and coworkers [50] using acid-catalyzed cohydrolysis method display a large surface area (Fig. 3c) and the addition of titanium results in less micropores (Fig. 3d) along with an increase in the pore diameter and pore volume as shown in Fig. 3e and f, respectively. The aerogels prepared by base-catalyzed, cohydrolysis method generally have smaller surface area, pore diameter and pore volume, and contain a greater proportion of micropores compared to the samples prepared by acid-catalyzed cohydrolysis method (cf. Fig. 3c–f).

The success of the new synthesis method relies on adjusting the reactions of the two alkoxide precursors to a comparable rate. The two-step, acid–base catalyzed method involves the acid prehydrolysis of the silicon alkoxide (i.e., TMOS) to generate reactive monomers and speed up its reaction. Using acetylacetone stabilized titanium precursor and carrying out the reaction under alkaline pH prevent the rapid hydrolysis and condensation of the titanium alkoxide. This results in the formation of a robust

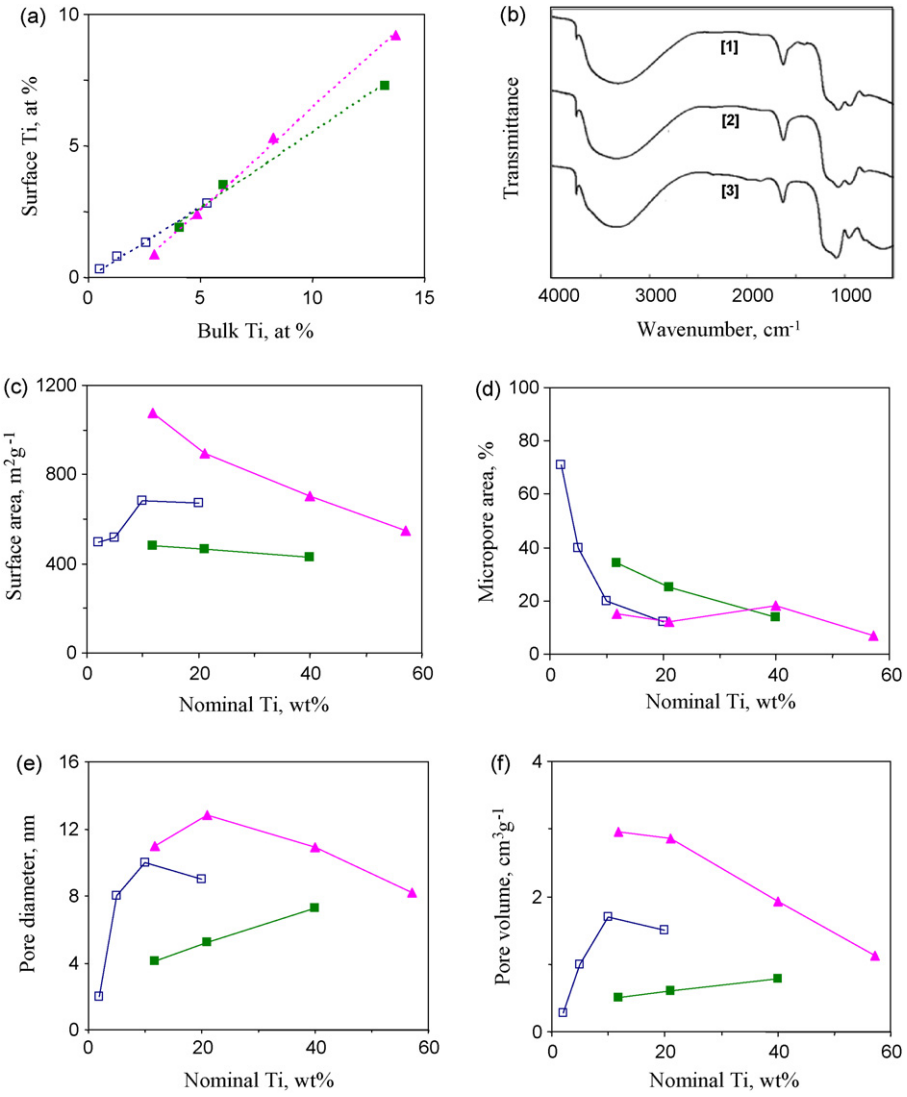

Fig. 3. Plots of (a) surface versus bulk Ti concentration, (b) infrared spectra, (c) BET surface area, (d) percent contribution from micropore area, (e) average pore diameter, and (f) total pore volume of titania–silica aerogels of different titanium content prepared by acid-catalyzed, cohydrolysis method (□, Baiker and coworkers [50]), base-catalyzed, co-hydrolysis method (■), and two-step, acid–base method (▲).

silica–titania gel network and crack-free aerogel that possesses enormous surface area and pore volume (cf. Fig. 3c and f). Among the three synthesis methods, it produces aerogels with the largest average pore diameter (Fig. 3e) and the least amount of micropores (Fig. 3d). In contrast to the other two methods, the addition of titanium led to a decrease in the aerogel surface area, pore diameter and pore volume.

Fig. 4a displays the SEM pictures of titania–silica aerogels prepared by the two-step, acid–base catalyzed method. The micrographs of the fractured aerogel samples show the clusters that made up the aerogel network. It can be seen from the figures that the clusters decrease in size with the addition of titanium and is consistent with the smaller pore diameter measured by nitrogen physisorption. The X-ray diffractograms in Fig. 4b indicate that anatase TiO_2 were crystallized after ethanol supercritical drying. The brookite or rutile phases were not detected. The high temperature, supercritical drying process promotes esterification, alcoholysis and dehydration reactions in the alcogel causing dissolution [54] and rearrangement of the gel network [50]. The water generated by alcohol dehydration is believed to be partly responsible for the rapid crystallization of anatase TiO_2 [55]. More crystalline samples (Fig. 4b) as well as larger TiO_2 crystals (Fig. 4c) were obtained from aerogels with higher titanium content.

The 2-propanol dehydration reaction carried out on pure anatase TiO_2 samples in Fig. 5a shows a direct linear dependence between the dehydration rate and anatase TiO_2 surface area. Following the same procedure described by Hanprasopwattana et al. [40], the surface area of the anatase TiO_2 in the titania–silica aerogels was calculated from the 2-propanol dehydration rate and plotted as a function of nominal Ti/Si ratio in Fig. 5b. The anatase TiO_2 crystallized in aerogel with dilute titanium content are small and poorly crystallized (cf. Fig. 4b). This could explain the smaller surface area (i.e., 90 $m^2\,g^{-1}$) measured by the probe reaction. Better crystallized TiO_2 obtained from more concentrated aerogel network displays a large surface area (i.e., 300–400 $m^2\,g^{-1}$). The UV–vis spectra of silica and titania–silica aerogels are shown in Fig. 5c. The UV absorbance at 365 nm is low for the silica aerogel and high for titania–silica aerogel. The UV penetration depth was measured according to the procedure described by Dreyer [43] and plotted in Fig. 5d. The UVA can penetrate deeper into the samples with low titanium compared with samples with high titanium content as one expects. A deeper UV penetration into the aerogel

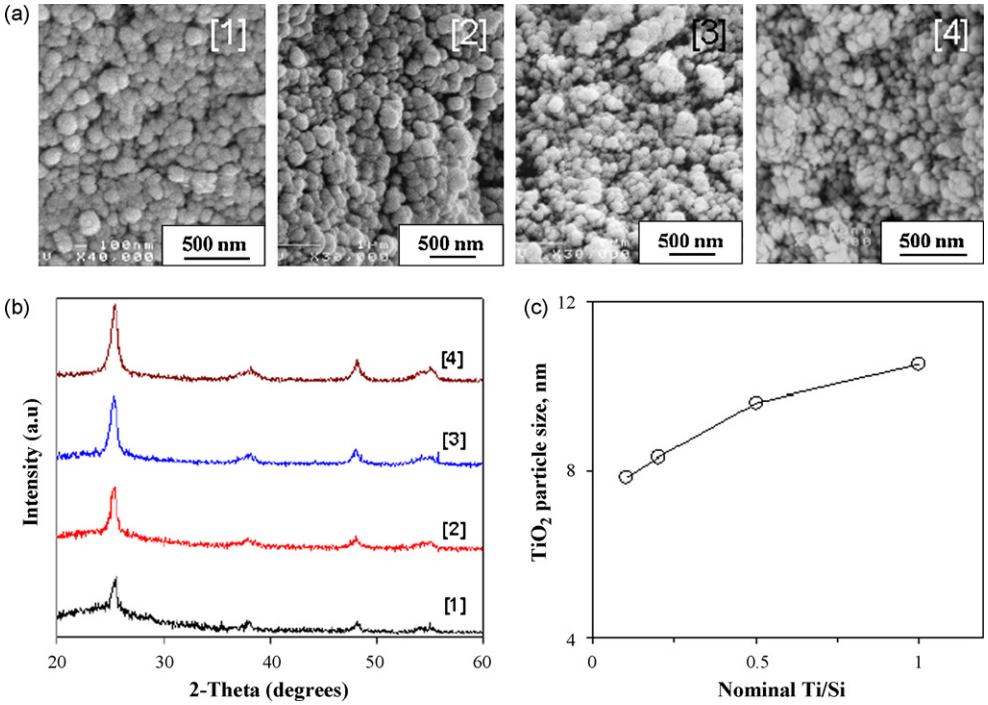

Fig. 4. (a) Scanning electron micrographs, (b) X-ray diffractograms and (c) anatase TiO_2 particle size of titania–silica aerogels containing [1] Ti/Si = 0.1 (TS01), [2] Ti/Si = 0.2 (TS02), [3] Ti/Si = 0.5 (TS05) and [4] Ti/Si = 1 (TS1) prepared by the two-step, acid–base method.

means a larger reactive volume that could lead to higher photon utilization efficiency.

Unlike traditional aerogels, the aerogels prepared by the two-step, acid–base catalyzed method are accessible to gases. Reports showed that silica aerogels have low permeability to gases with fluxes in the order of $\mu l\ min^{-1}$ [38,39]. Fig. 6a plots the pressure drop across the aerogel as a function of oxygen flow. The traditional silica aerogel as reported by Hosticka et al. [39] is nearly impermeable to gases and is characterized by low flux and high pressure drop as shown in Fig. 6a-(1), while the silica aerogel prepared in this work (Fig. 6a-(5)) is able to sustain a four orders of magnitude higher flux at a comparable pressure drop. The addition of titanium into the aerogel matrix resulted in higher transport resistance consistent with the observed decrease in the pore diameter and pore volume. Oxygen diffusion through the aerogel was measured and plotted in Fig. 6b for the different aerogels. Oxygen diffusion through the silica and titania–silica (Ti/Si = 0.2, 0.5 and 1) aerogels displays a temperature dependence of $T^{1.44}$,

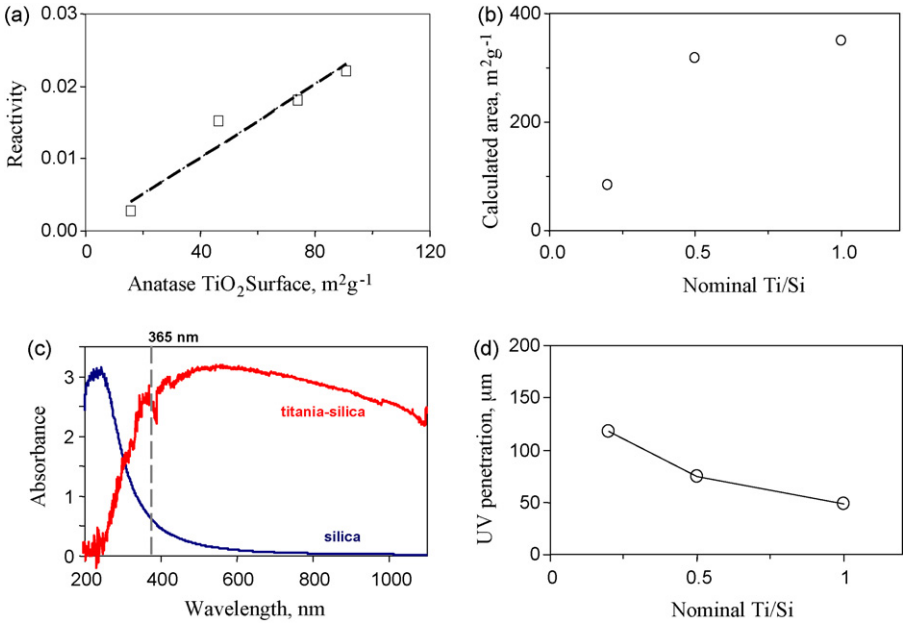

Fig. 5. (a) IPA dehydration rate at 533 K over reference anatase TiO_2 and (b) calculated anatase TiO_2 surface area of titania–silica aerogels with different nominal Ti/Si ratios prepared by the two-steps, acid–base method. (c) UV–vis spectra of pure silica and titania–silica aerogels and (d) calculated UV penetration depth (710 $\mu W\ cm^{-2}$, 365 nm) in titania–silica samples with different titanium contents.

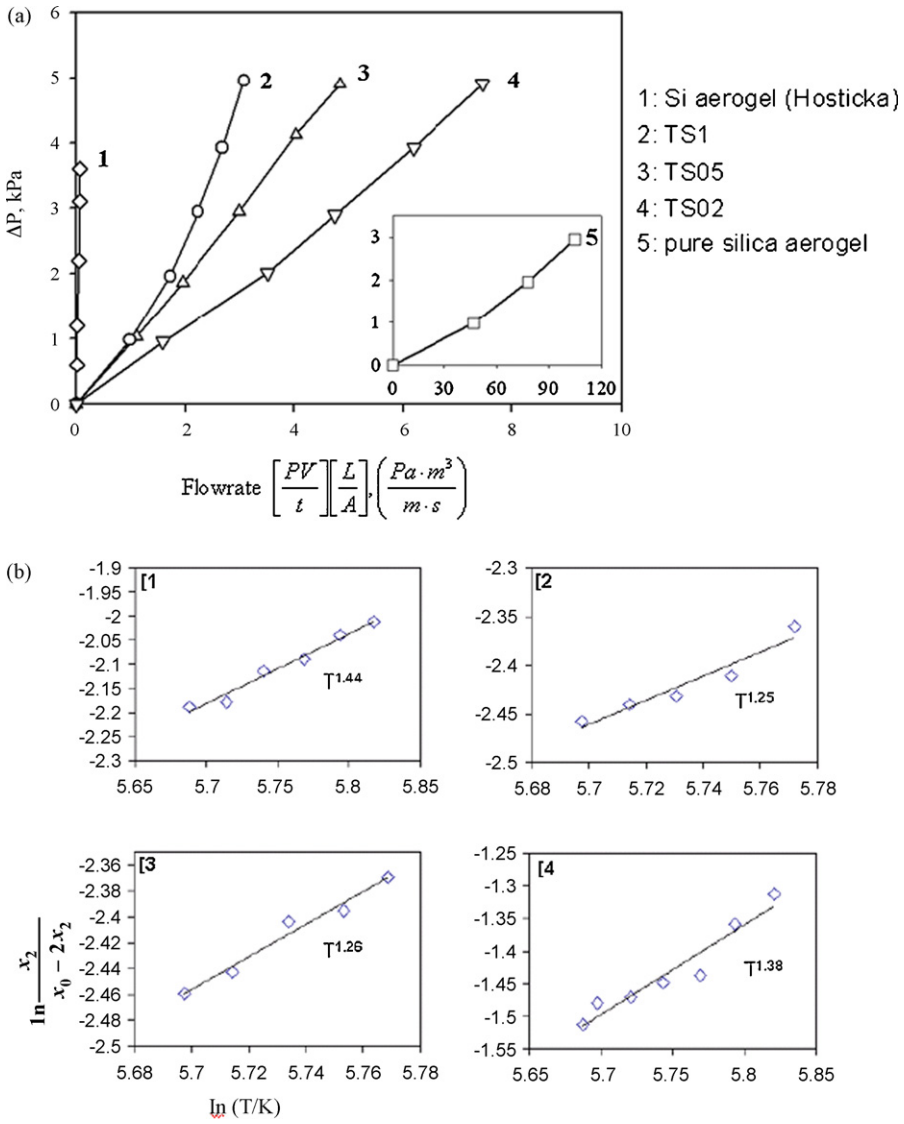

Fig. 6. (a) Plots of pressure drop as a function of gas flow through the aerogel at 300 K and 101 kPa. (Note: O_2 was used in this work and N_2 was used by Hosticka et al. [39]). (b) O_2 diffusion measurement for silica and titania–silica aerogels (T is the temperature; x_0 is the inlet O_2; x_2 is the outlet O_2.)

$T^{1.25}$, $T^{1.26}$ and $T^{1.38}$, respectively. This suggests a transition regime diffusion between Knudsen (i.e, $T^{0.5}$) and molecular (i.e., $T^{1.5}$) diffusion that is common in mesoporous materials.

3.2. Performance of catalytic aerogel filters

The silica and titania–silica aerogels prepared by the two-step, acid–base catalyzed method were tested for aerosol and bioaerosol filtrations, PCO reaction and bactericidal activity.

Aerosol and bioaerosol filtrations were carried out on silica (i.e., S_HT) and titania–silica (i.e., TS01 and TS1) aerogels. Guise et al. [56] reported the use of a packed bed of SiO_2 aerogel microspheres to capture 20–2000 nm airborne particles. Aerosol and bioaerosol are captured in porous matrix by Brownian diffusion, direct interception and inertial impaction [56]. Particles smaller than 0.3 μm are removed by Brownian diffusion, while the larger particles are captured by direct interception and inertial impaction. The capture of 0.3 μm aerosol is often the least efficient and is used as a measure of filtration efficiency. Table 1 shows that roughly a third of the aerosol oil droplets were captured as it filtered through the 7 mm thick silica aerogel that has a 30 nm pore diameter. Twice the amount of aerosol oil droplets (ca. 65%) was captured by the 7.5 mm TS01 titania–silica aerogel that has 11 nm pores. TS01s smaller pores and denser network were believed to be responsible for the improved aerosol filtration. The results show that the aerogels are able to filter aerosols, but at a lower efficiency compared to the commercial HEPA filters rated to remove 99.99% of the 0.3 μm aerosol. However, it must be admitted that the prepared aerogels were not optimized for aerosol filtration.

Table 1
Aerosol filtration by aerogel filters

Sample	Air flow (sccm)	Time (min)	Aerosol in (mg)	Aerosol out (mg)	Aerosol removed (%)
S_HT[a]	192	60	26.26	18.00	32
	162	60	19.13	13.21	31
TS01[b]	202	60	33.29	9.36	72
	210	60	17.9	7.4	58

[a] Silica aerogel (S_HT) has a diameter of 16 mm and thickness of 7 mm.
[b] Titania–silica aerogel (TS01 raw) has a diameter of 14 mm and thickness of 7.5 mm.

Table 2
Bioaerosol filtration by aerogel filters

Sample	Air flow (sccm)	Bioaerosol in (CFU/m^3)	Bioaerosol out (CFU/m^3)	Bioaerosol removed (%)
S_HT[a]	200	750	125	83
TS1[b]	200	667	42	94

[a] Silica aerogel (S_HT) has a diameter of 16 mm and thickness of 7 mm.
[b] Titania–silica aerogel (TS1) has a diameter of 11 mm and thickness of 3 mm.

Table 3
Properties of titania–silica aerogels used for the photocatalytic oxidation of TCE

Sample	Nominal Ti/Si	Surface area (m^2/g)	TiO_2 loading (mg)	TiO_2 crystal size (nm)	Anatase TiO_2 surface area (m^2)	Dimensions *d* and *h* (mm)
TS02	0.2	900	28	8.3	13	12.5, 4.5
TS05	0.5	700	48	9.6	50	12.0, 4.0
TS1	1.0	550	55	10.5	40	11.0, 3.0

Microorganisms are ubiquitous in the environment and indoor air contains airborne bacteria and spores as well as pollens among other bioaerosols. The indoor air was filtered through the aerogels and the bacteria removed were reported in Table 2. No attempt was made to identify the bacteria species present in the indoor air and both the fungi and mold spores present in the air were excluded from the study. Greater than 80% of the natural airborne bacteria were filtered from the indoor air by the silica aerogel (i.e., S_HT), while better than 90% were removed by the TS1 aerogel despite being much thinner (i.e., 3 mm versus 7 mm). The higher removal rate is due to the larger size of the bacteria compared to the 0.3 μm test aerosol oil droplets and the bacteria were captured mainly by direct interception and inertial impaction on the aerogel network.

Photocatalytic oxidation reaction was carried out in the aerogel photoreactor for trichloroethylene (TCE) in air. The reactant mixture flowed through the freestanding block of aerogel catalyst while being irradiated by a single fluorescent black lamp (i.e., 365 nm, 710 μW/cm^2). To eliminate the effect of mass transport, the reaction was conducted at a reactant flow of 40 sccm [36]. The silica aerogel (S_HT) was inactive for photocatalytic oxidation of TCE. It was also established that titania–silica aerogel containing only Ti–O–Si sites without anatase TiO_2 is also inactive for the reaction [35]. Fig. 7a plots the reaction rate as a function of TCE feed concentration for TS02, TS05 and TS1 aerogels. No toxic intermediates and byproducts such as dichloroacetaldehyde, dichloroacetyl chloride and phosgene were detected in the reaction. The aerogel catalysts were stable and did not deactivate during 180 h of reaction. The plots in Fig. 7a do not show a consistent trend, and could be attributed to the difference in the Ti loading, mass and size of the aerogel catalysts used in the reaction (cf. Table 3). The TCE conversion rate of TS1 is 9.2×10^{-5} mmol s^{-1} g^{-1} compared to the same catalyst in a flat plate reactor of 4.3 10^{-5} mmol s^{-1} g^{-1} [34]. Degussa P25 TiO_2 powder was also tested in the flat plate reactor and had a TCE conversion rate of 5.1×10^{-6} mmol s^{-1} g^{-1}. This shows that TS1 is an order of magnitude more reactive than the commercial catalyst.

Fig. 7b plots the turnover number (TON) calculated based on the total titanium content of the aerogels, i.e., including anatase TiO_2, amorphous titania and Ti–O–Si network. The plots show that TS02 has the highest TON followed by TS1 and TS05. A similar trend was obtained from the plots of turnover frequency (TOF) as shown in Fig. 7c. The TOF was calculated based on the anatase TiO_2 surface area (cf. Fig. 5b) determined from 2-propanol dehydration reaction according to the method of Hanprasopwattana et al. [40]. Furthermore, if the reactive volume is calculated based on the UV penetration data in Fig. 5d, it is possible to obtain Fig. 7d. The plots in Fig. 7d take into account that only the illuminated portion of the aerogel participates in the PCO reaction. The reaction results indicate that TS02 is the most active for the photocatalytic oxidation of TCE. The anatase TiO_2 in TS02 measures 8 nm in diameter, which is close to the optimum size of 7 nm found in the previous study of TCE photocatalytic oxidation over anatase TiO_2 [23] and could explain its higher reactivity. In addition, the faster gas transport rate in TS02 would also favor a faster reaction. An increase in the titanium content of the aerogels results in larger anatase TiO_2 particles (cf. Fig. 4c) and a marked change in the

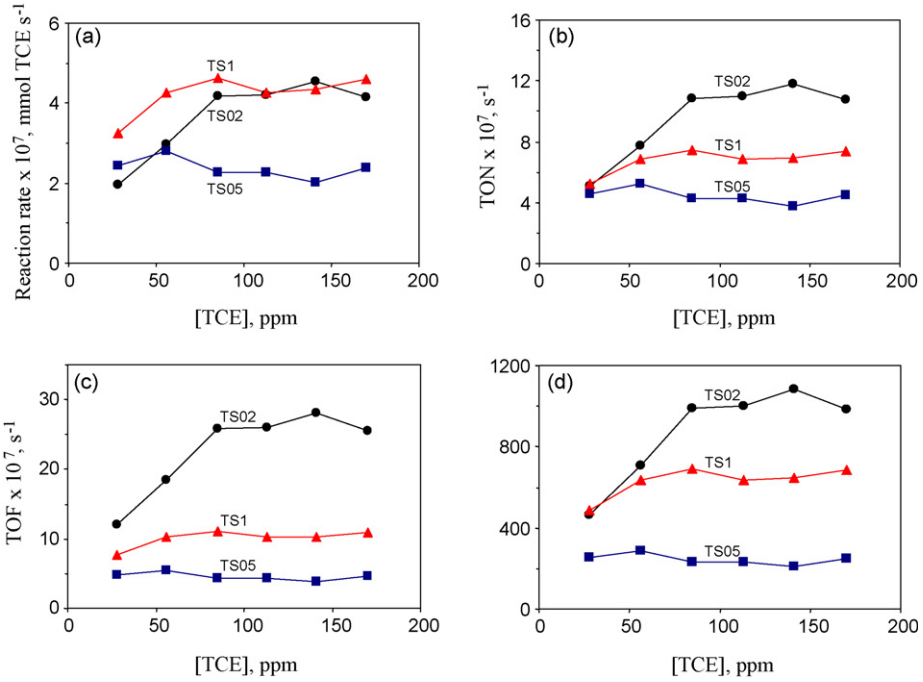

Fig. 7. Plots of the (a) reaction rate, (b) TON based on the total titanium, (c) TOF based on the anatase TiO_2 surface and (d) TOF accounting for the reactive volume for TCE photocatalytic oxidation on titania–silica aerogels containing Ti/Si = 0.2 (TS02), Ti/Si = 0.5 (TS05) and Ti/Si = 1 (TS1).

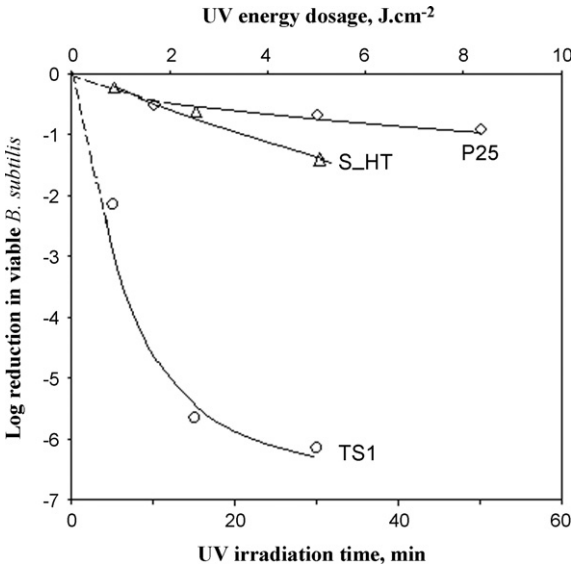

Fig. 8. Log reduction in viable *B. subtilis* on Degussa P25 TiO_2, TS1 and S_HT following exposure to UVA (710 μW/cm^2).

textural property of the materials (cf. Figs. 3c–e) leading to lower gas permeability (cf. Fig. 6) and UV transparency (cf. Fig. 5d). TS1 was able to compensate by having higher TiO_2 loading and thus display better activity than TS05.

Bactericidal activity of commercial Degussa P25 and TS1 was measured for *B. subtilis* cells and the results are shown in Fig. 8. The viable bacteria decrease with UVA irradiation as shown in the figure. The P25 TiO_2 displays a modest bactericidal activity and displays a log reduction of 0.9 (i.e., 83% kill) after exposure to UVA for 50 min (365 nm, 8.5 J/cm^2) while a 6 log reduction or 99.9999% kill was obtained from TS1 at a shorter UVA exposure time of 30 min (4 J/cm^2). A glass plate (i.e., control sample) irradiated for 50 min shows a much smaller 0.15 log (29%) decrease in viable *B. subtilis* cells. It is speculated that the exceptionally high bactericidal activity of TS1 originates from the greater number of reactive oxygen species (ROS) generated during UVA irradiation of the aerogel. Unlike P25 TiO_2, ROS are produced not only by the anatase TiO_2 crystals in TS1 but also by the Ti–O–Si and Si–O–Si aerogel networks. Evidence for the latter could be seen from bactericidal activity of UVA irradiated silica aerogel in Fig. 8 and observed reactivity of Ti–O–Si and Si–O–Si for partial oxidation reactions [35]. Other researchers also reported that UV irradiated nano-sized SiO_2 is active against *B. subtilis* and *E. coli* [57]. ROS can damage cell membrane by lipid peroxidation resulting in a change of membrane permeability and fluidity making the cell less able to absorb nutrient and more vulnerable to osmotic stress [58]. Aldehydes produced by the peroxidation reaction could further damage proteins and other cell components. ROS also damage DNA by direct reaction with the nucleic acids [58,59]. The enormous charged surface of the aerogel is also a contributing factor to its effectiveness against bacteria. Contact with the charged surfaces is known to interfere with the membrane function and interrupt energy transduction [60]. Thus, the aerogel represents a hostile environment for the microorganisms and this could explain the absence of viable bacteria from the aerogel blocks recovered from the bioaerosol filtration experiments.

4. Concluding remarks

The freestanding crack-free titania–silica aerogels prepared by the two-steps acid–base catalyzed method are gas permeable and photoactive. The aerogel blocks are of adequate strength (i.e., up to 40 kN m^{-2}) to withstand normal handling and processing. The photoactive anatase TiO_2 nanoparticles crystallized within the aerogel are trapped by the porous silica network. This prevents their accidental release into the environment and avoids the potential adverse health and environmental impacts suggested in recent studies [61–63]. The porous aerogel network could also trap and filter airborne particulates and the titania–silica aerogel has a fair performance for aerosol (65%) and bioaerosol (94%) filtrations in comparison to commercial HEPA filters (99.99%). The titania–silica aerogels are excellent photocatalysts being an order of magnitude more active than the commercial Degussa P25 TiO_2 for photooxidation of TCE and six orders of magnitude greater bactericidal activity against *B. subtilis* cells than the Degussa P25 TiO_2. This suggests that further study to improve aerogel permeability and possibly particulate filtration is worthwhile. High material and processing cost remains an obstacle in developing self-supporting, catalytic aerogel filters. Advances in processing technology including rapid supercritical extraction process using hydraulic press reactors could halves the processing cost and time [64]. Thin film coating on filter substrates could prove to be a more cost effective way of obtaining high efficiency catalytic filter that has the superior photocatalytic and germicidal properties of titania–silica aerogel and the excellent filtration efficiency of a HEPA filter. The mixed-oxides aerogels are also attractive support for metal catalysts including gold catalysts for CO remediation [65,66].

Acknowledgements

The authors would like to thank the financial support from the Hong Kong Research Grant Council and the Hong Kong Innovation and Technology Commission. We also thank the technical help from the Material Preparation and Characterization Facility (MCPF) and the Advanced Engineering Material Facility (AEMF) of the Hong Kong University of Science and Technology.

References

[1] A. Mills, S. LeHunte, J. Photochem. Photobiol. A 108 (1997) 1–35.
[2] J. Peral, D.F. Ollis, J. Catal. 136 (1992) 554–565.
[3] R.M. Alberici, W.F. Jardim, Appl. Catal. B-Environ. 14 (1997) 55–68.
[4] K.P. Yu, W.M. Lee, W.M. Huang, C.C. Wu, C.L. Lou, S.H. Yang, J. Air Waste Manage. 56 (2006) 666–674.
[5] A. Vohra, D.Y. Goswami, D.A. Deshpande, S.S. Block, Appl. Catal. B-Environ. 64 (2006) 57–65.
[6] C.Y. Lin, C.S. Li, Aerosol Sci. Technol. 37 (2003) 939–946.
[7] Y. Kikuchi, K. Sunada, T. Iyoda, K. Hashimoto, A. Fujishima, J. Photochem. Photobiol. A 106 (1997) 51–56.
[8] K. Sunada, T. Watanabe, K. Hashimoto, J. Photochem. Photobiol. A 156 (2003) 227–233.
[9] C.R. Bickmore, K.F. Waldner, R. Baranwal, T. Hinklin, D.R. Treadwell, R.M. Laine, J. Eur. Ceram. Soc. 18 (1998) 287–297.
[10] C.B. Almquist, P. Biswas, J. Catal. 212 (2002) 145–156.
[11] L.K. Campbell, B.K. Na, E.I. Ko, Chem. Mater. 4 (1992) 1329–1333.
[12] V. Strengl, S. Bakardjieva, J. Subrt, J. Szatmary, Micropor. Mesopor. Mater. 91 (2006) 1–6.
[13] J.M. Watson, A.T. Cooper, J.R.V. Flora, Environ. Eng. Sci. 22 (2005) 666–675.
[14] G. Dagan, M. Tomkiewicz, J. Non-Cryst. Solids 175 (1994) 294–302.
[15] S. Yoda, D.J. Suh, T. Sato, J. Sol–Gel Sci. Technol. 22 (2001) 75–81.
[16] J. Joo, S.G. Kwon, T. Yu, M. Cho, J. Lee, J. Yoon, T. Hyeon, J. Phys. Chem. B 109 (2005) 15297–15302.
[17] X. Peng, A. Chen, J. Mater. Chem. 14 (2004) 2542–2554.
[18] P. Hoyer, Langmuir 12 (1996) 1411–1413.
[19] Z.Y. Yuan, B.L. Su, Colloid Surf. A 241 (2004) 173–183.
[20] C. Aprile, A. Corma, H. Garcia, Phys. Chem. Chem. Phys. 10 (2008) 769–783.
[21] M. Qamar, C.R. Yoon, H.J. Oh, N.H. Lee, K. Park, D.H. Kim, K.S. Lee, W.J. Lee, S.J. Kim, Catal. Today 131 (2008) 3–14.
[22] M. Wu, G. Li, D. Chen, G. Wang, D. He, S. Feng, R. Xu, Chem. Mater. 14 (2002) 1974–1998.
[23] A.J. Maira, K.L. Yeung, C.Y. Lee, P.L. Yue, C.K. Chan, J. Catal. 192 (2000) 185–196.
[24] A.J. Maira, K.L. Yeung, J. Soria, J.M. Coronado, C. Belver, C.Y. Lee, V. Augugliaro, Appl. Catal. B 29 (2000) 327–336.

[25] A.J. Maira, J.M. Coronado, V. Augugliaro, K.L. Yeung, J.C. Conesa, J. Soria, J. Catal. 202 (2001) 413–420.
[26] J.M. Coronado, A.J. Maira, J.C. Conesa, K.L. Yeung, V. Augugliaro, J. Soria, Langmuir 17 (2001) 5368–5374.
[27] D.M. Antonelli, J.Y. Ying, Angew. Chem. Int. 34 (1995) 2014–2017.
[28] F. Bosc, A. Ayral, P.A. Albouy, L. Datas, C. Guizard, Chem. Mater. 16 (2004) 2208–2214.
[29] J.G. Yu, J.C. Yu, W.L.K. Ho, Z.T. Jiang, New J. Chem. 26 (2002) 607–613.
[30] Y. Yamauchi, F. Takeuchu, S. Todoroki, Y. Sakka, S. Inoue, Chem. Lett. 37 (2008) 72–73.
[31] S. Yoda, K. Ohtake, Y. Takebayashi, T. Sugeta, T. Sako, J. Sol–Gel Sci. Technol. 19 (2000) 719–723.
[32] S. Yoda, K. Ohtake, Y. Takebayashi, T. Sugeta, T. Sako, T. Sato, J. Mater. Chem. 10 (2000) 2151–2156.
[33] W. Kim, I.K. Hong, J. Ind. Eng. Chem. 9 (2003) 728–739.
[34] S. Cao, K.L. Yeung, P.L. Yue, Appl. Catal. B-Environ. 68 (2006) 99–108.
[35] S. Cao, K.L. Yeung, P.L. Yue, Appl. Catal. B-Environ. 76 (2007) 64–72.
[36] S. Cao, N. Yao, K.L. Yeung, J. Sol–Gel Sci. Technol. (2008) 1–11.
[37] S. Cao, K.L. Yeung, P.L. Yue, Stud. Surf. Sci. Catal. 159 (2006) 465–468.
[38] J. Phalippou, G.W. Scherer, T. Woignier, D. Bourret, R. Sempere, J. Non-Cryst. Solids 186 (1995) 64–72.
[39] B. Hosticka, P.M. Norris, J.S. Brenizer, C.E. Daitch, J. Non-Cryst. Solids 225 (1998) 293–297.
[40] A. Hanprasopwattana, S. Srinivasan, A.G. Sault, A.K. Datye, Langmuir 12 (1996) 3173–3179.
[41] K.L. Yeung, A.J. Maira, J. Stolz, E.W.C. Hung, N.K.C. Ho, A.-C. Wei, J. Soria, K.-J. Chao, P.-L. Yue, J. Phys. Chem. B 106 (2002) 4608–4616.
[42] K.L. Yeung, S.T. Yau, A.J. Maira, J.M. Coronado, J. Soria, P.L. Yue, J. Catal. 219 (2003) 107–116.
[43] M. Dreyer, Titanium dioxide aerogels as photocatalysts for indoor air decontamination, Thesis (Ph. D.), University of Oklahoma, 2002.
[44] M.M. van Bommel, B.B. de Haan, J. Mater. Sci. 29 (1994) 943–950.
[45] A.V. Rao, N.N. Parvathy, J. Mater. Sci. 28 (1993) 3021–3026.
[46] A.R. Rao, G.M. Pajonk, N.N. Parvathy, J. Mater. Sci. 29 (1994) 1807–1817.
[47] M. Schneider, A. Baiker, J. Mater. Chem. 2 (1992) 587–589.
[48] C.J. Brodsky, E.I. Ko, J. Mater. Chem. 4 (1994) 651–652.
[49] M. Schneider, A. Baiker, Catal. Today 35 (1997) 339–365.
[50] D.C.M. Dutoit, M. Schneider, A. Baiker, J. Catal. 153 (1995) 165–176.
[51] D.C.M. Dutoit, U. Gobel, M. Schneider, A. Baiker, J. Catal. 164 (1996) 433–439.
[52] M. Schneider, A. Baiker, Catal. Rev. -Sci. Eng. 37 (1995) 515–556.
[53] J.B. Miller, S.T. Johnston, E.I. Ko, J. Catal. 150 (1994) 311–320.
[54] S. Yoda, S. Ohshima, J. Non-Cryst. Solids 248 (1999) 224–234.
[55] S.J. Teichner, G.A. Nicolaon, M.A. Bicarini, G.E.E. Gardes, Adv. Colloid Interface 5 (1976) 245–273.
[56] M.T. Guise, B. Hosticka, B.C. Earp, P.M. Norris, J. Non-Cryst. Solids 285 (2001) 317–322.
[57] L.K. Adams, D.Y. Lyon, P.J.J. Alvarez, Water Res. 40 (2006) 3527–3532.
[58] E. Cabiscol, J. Tamarit, J. Ros, Int. Microbiol. 3 (2000) 3–10.
[59] J.A. Imlay, Ann. Rev. Microbiol. 57 (2003) 395–418.
[60] T. Mashino, K. Okuda, T. Hirota, M. Hirobe, T. Nagano, M. Mochizuki, Bioorg. Med. Chem. Lett. 9 (1999) 2959–2962.
[61] J.R. Gurr, A.S.S. Wang, C.H. Chen, K.Y. Jan, Toxicology 213 (2005) 66–73.
[62] T.C. Long, N. Saleh, R.D. Tilton, G.V. Lowry, B. Veronesi, Environ. Sci. Technol. 40 (2006) 4346–4352.
[63] B. Nowack, T.D. Bucheli, Environ. Pollut. 150 (2007) 5–22.
[64] B.M. Gauthier, S.D. Bakrani, A.M. Anderson, M.K. Caroll, J. Non-Crystal. Sol. 350 (2004) 238–243.
[65] K.Y. Ho, K.L. Yeung, Gold Bull. 40 (2007) 15–30.
[66] K.Y. Ho, K.L. Yeung, J. Catal. 242 (2006) 131–141.